

**Femtosecond Raman Microscopy Reveals Structural Dynamics Leading to Triplet
Separation in Rubrene Singlet Fission**

Supporting Information

Kajari Bera, Christopher J. Douglas and Renee R. Frontiera*

*To whom correspondence should be addressed. rrf@umn.edu, 612-624-2501

Experimental Methods:

Sample preparation: We used $\geq 98\%$ purity rubrene powder from Sigma Aldrich and grew the rubrene crystals using the previously reported methods of physical vapor transport.^{1,2} We heated the furnace overnight at $350\text{ }^{\circ}\text{C}$ before the crystal growth to minimize impurity content. We then placed 16 mg of rubrene powder in a glass boat inside the furnace in the presence of 0.1 MPa Argon gas with a flow rate of 100 ml/min for 90 minutes to create an inert atmosphere. We heated the furnace to $330\text{ }^{\circ}\text{C}$ at the source region by a thermocouple for 35 min and the crystals were formed 5-8 cm away from the source region. We obtained long needle-shaped orange colored rubrene crystals, 4-6 mm long, and then mounted them onto glass slides. F₂₀ rubrene was prepared according to our previously reported route.³

UV-visible spectroscopy: We obtained the absorption spectrum of rubrene crystals using UV-2600 UV-Vis spectrophotometer by Shimadzu in transmission mode.

Continuous wave Raman spectra: We obtained the spontaneous Raman spectra of rubrene crystals and F₂₀ rubrene powder using a home-built Raman spectrometer. We passed a 785 nm laser through a 30:70 beam splitter and focused onto the sample through a 10x Olympus objective. The power of the laser at the sample was 21 mW and we collected the Raman signal in a back-scattering geometry using a Princeton Instruments 2500i spectrograph and a Princeton Instruments PIXIS 100BX CCD array.

Femtosecond stimulated Raman spectroscopy: We collected the time-resolved Raman data on a home-built setup which employed Coherent model Libra-F-1K-HE-110 femtosecond amplifier.⁴ The 4.6 W fundamental output at 800 nm was used to generate the three pulses for the FSRS studies. We passed 480 mW of the fundamental output beam through our home-built grating

filter to generate a 2.1 ps narrowband Raman pump.⁵ We generated the broadband continuum femtosecond Raman probe by passing 2.5 mW of the 800 nm fundamental output through a 2 mm thick sapphire crystal followed by a RG830 long pass filter and then compressed it with a fused silica prism compressor. The photoexcitation pump was generated by a home-built non-collinear parametric amplifier (NOPA). NOPA generation required a seed pulse and a 400 nm pump pulse. The white light seed continuum was generated in a 2 mm thick sapphire crystal. The 400 nm pump pulse was generated by frequency doubling the 800 nm fundamental output using a BBO crystal. The two pulses were then mixed in a 1 mm thick BBO crystal and the resultant visible light was passed through an SF10 prism compressor to minimize the linear chirp. The photoexcitation pump was tuned to a central wavelength of 536 nm and a FWHM of 14 nm with a Gaussian spectral shape. We sent the three pulses through an inverted Olympus IX 73 microscope and focused them non-collinearly onto the sample using a 35 mm focal length lens. We used a piezoelectric stage to vary the time delay between the photoexcitation pump and the Raman pump-probe. The cross-correlation of the photoexcitation pump and the Raman probe was 250 ± 2 fs as measured by the optical Kerr effect with a 2 mm cuvette of cyclohexane. We focused the Raman probe and the stimulated Raman signal using a 100 mm focal length lens on to a 1/3 meter spectrograph and a Princeton Instruments PIXIS 100F CCD array that collected the spectra at a kHz repetition rate. We used a home-built Labview program to collect the femtosecond stimulated Raman spectrum where each spectrum was collected for 20-90 seconds and obtained the Raman gain spectra by dividing the Raman pump on spectra over Raman pump off spectra.

Low frequency Raman spectrum of crystalline rubrene:

We show the low frequency spontaneous Raman spectrum of the rubrene crystal used for FSRS in Figure S1. The low frequency Raman modes depicted in the figure correspond to the orthorhombic polymorph of crystalline rubrene.⁶ We use the low frequency Raman modes to determine the orientation of the crystal for the spontaneous Raman measurements. Comparing the frequencies and relative intensities of the phonon modes at 72, 104, 116 and 136 cm^{-1} with ref 6, we determine that the Raman excitation is normal to the *ab* face of the needle for the spontaneous Raman measurements.

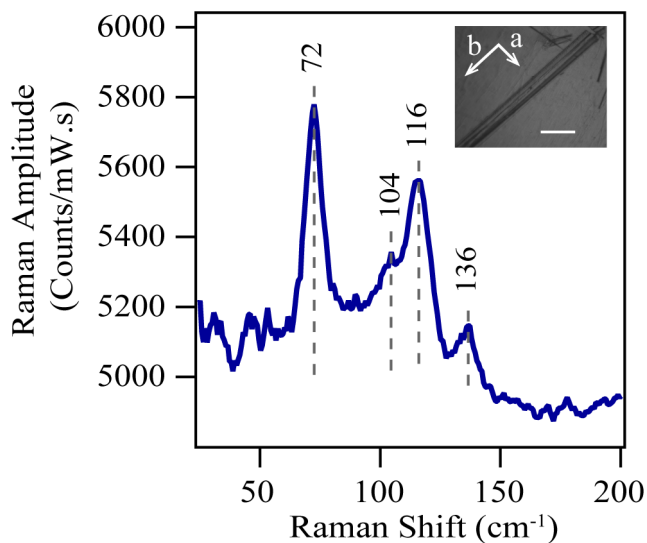


Figure S1. Low frequency Raman spectrum of a rubrene crystal (inset) with prominent peaks indicated by dashed lines. The scale bar is 0.4 mm in length.

Photoluminescence Spectrum:

We measured PL spectrum of the needle shaped rubrene crystal to verify if the crystal is pristine or not. We obtained the PL spectrum on the same continuous wave Raman set-up as described previously and plot the same in Figure S2. We collected the PL spectrum in 6 separate detection windows causing a slight overlap as visible in Figure S2. The absence of the 650 nm peak in our PL spectra indicates that we cannot detect any impurities.^{7,8}

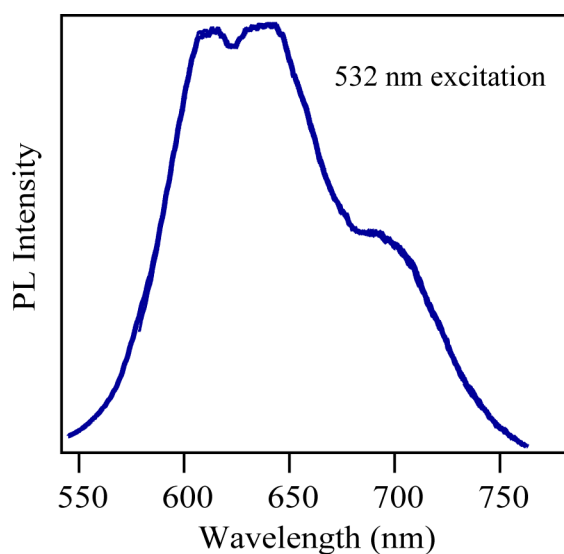


Figure S2. PL spectrum of the needle shaped crystalline rubrene. Absence of 650 nm peak implies that the crystal is pristine.

Photoexcitation pump profile:

The spectrum of the photoexcitation pump is shown in Figure S3.

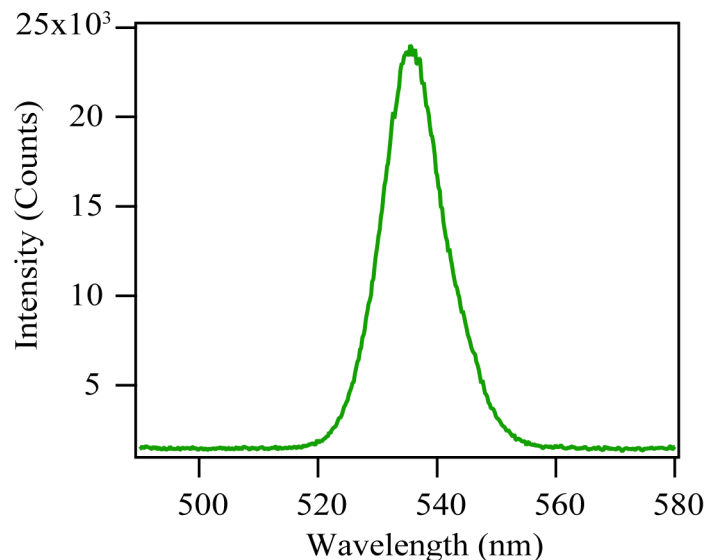


Figure S3. Spectral profile of the photoexcitation pump.

Raw FSR data of crystalline rubrene:

We plot the FSR data of crystalline rubrene after one to one subtraction of the excited state spectra from the ground state spectrum in Figure S4. The ground state Raman spectrum of rubrene has peaks at 1210, 1305 and 1434 cm^{-1} corresponding to C-C stretching motions in the tetracene backbone and C-H wagging motions in rubrene molecule according to our DFT calculations, and are depleted in amplitude following photoexcitation.

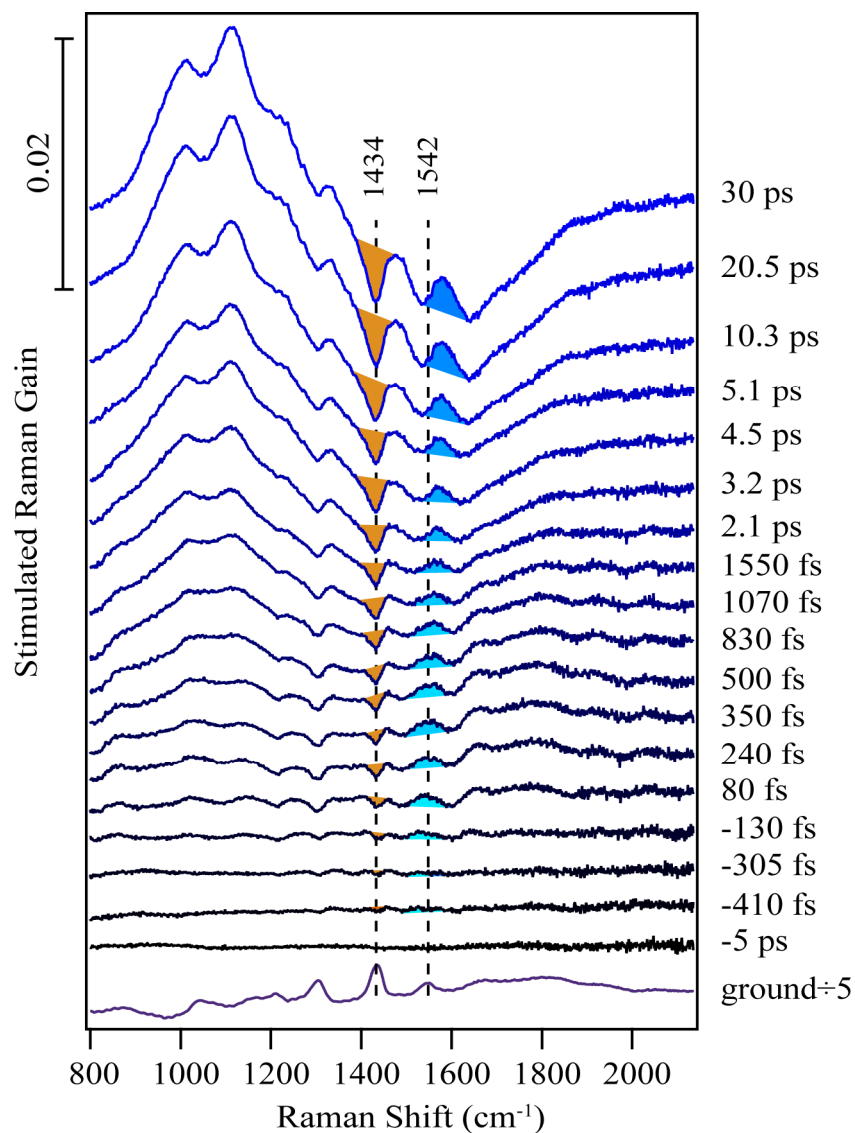


Figure S4. Raw FSR spectra of crystalline rubrene at various time delays after photoexcitation. The shaded region indicates the ground state depletion (brown) and one of the excited state features (blue).

Kinetics of ground state addition:

The large depletion of the ground state peaks in the excited state spectra demanded the addition of ground state spectrum to unambiguously examine the excited state dynamics. We add the ground state back to the excited state difference spectra until no negative features of any of

the ground state peaks are present. We show the spectra obtained after the addition of ground state to the excited state spectra in Figure 2 of the main text. Figure S5 shows the kinetics of the amount of ground state added back to the excited state spectrum, which is in agreement with the rapid formation of the correlated triplet pair and subsequent long-lived triplet states.

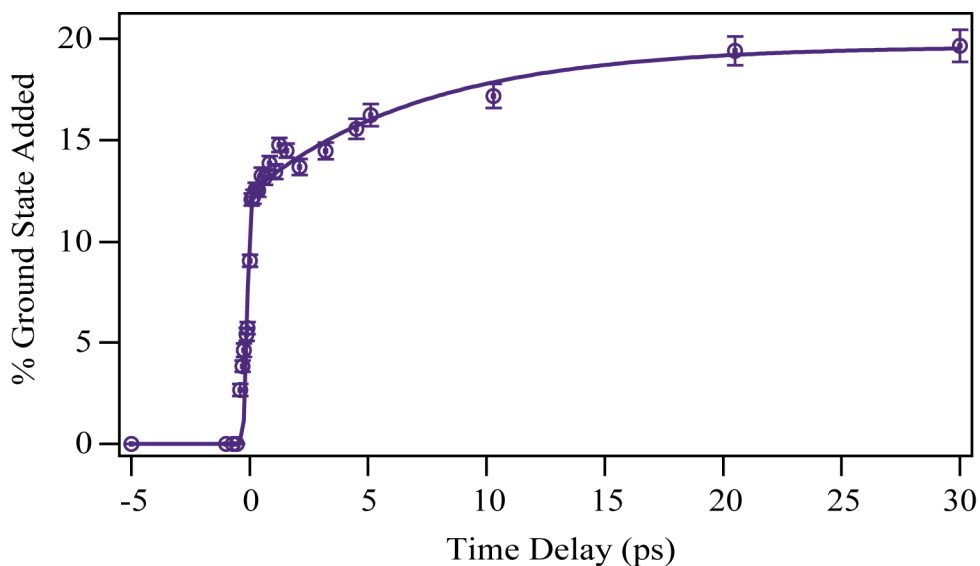


Figure S5. Time resolved kinetics of the percentage of ground state added back to the excited state spectra with corresponding exponential fit.

Transient absorption data of crystalline rubrene:

We plot the transient absorption spectra with the Raman pump off in Figure S6. The intensity of the 877 nm peak in the transient absorption increases as a function of time indicating it to be an excited state absorption feature. This peak in transient absorption corresponds to the 1117 cm^{-1} peak in FSRS from Figure 2.

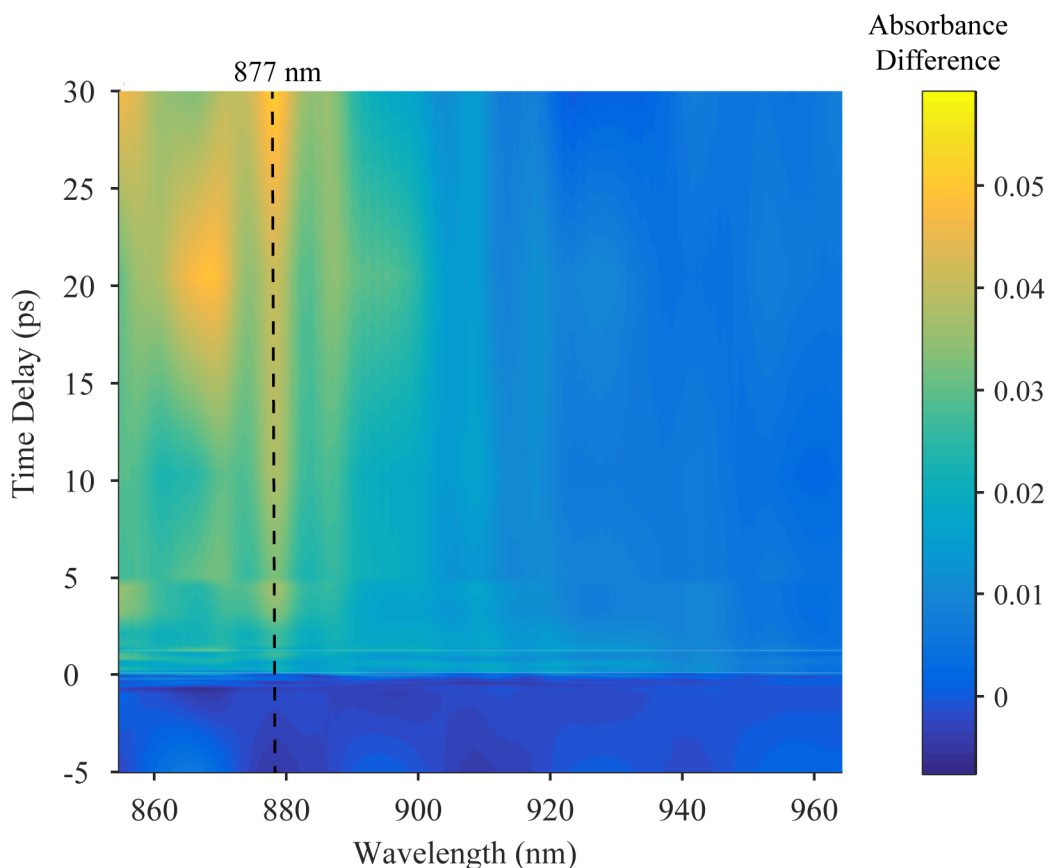


Figure S6. Transient absorption plot of rubrene crystal. The intensity of the peak at 877 nm increases with time indicating it to be an excited state absorption feature.

Excited state vibrational linewidths:

We fit the peaks around 1430 and 1542 cm^{-1} in Figure 2 from the main text to a single Gaussian with a linear baseline. The linewidths of the fit as a function of time is presented in Figure S7. We see no trend in the linewidths and thus this discards the possibility of vibrational cooling being the origin of the frequency evolution.

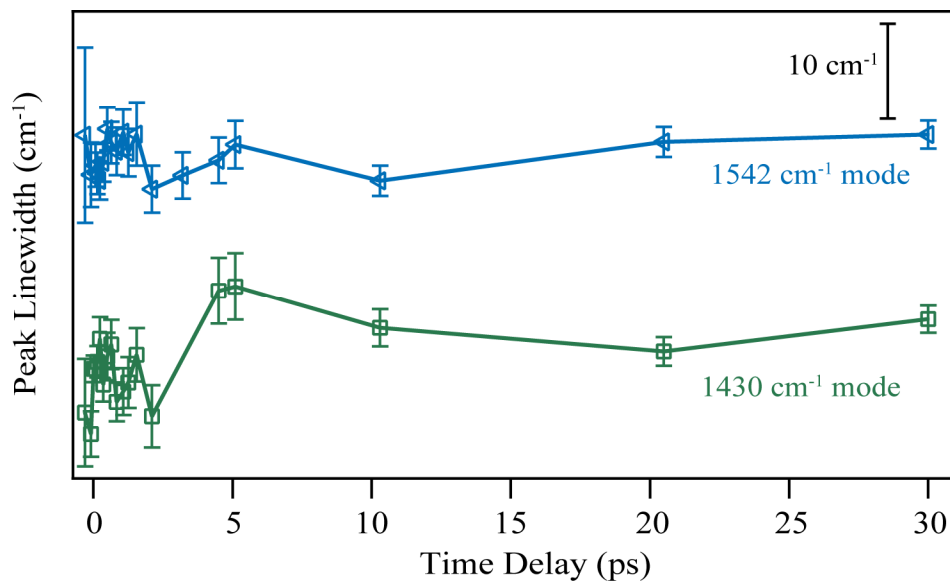


Figure S7. The linewidths obtained from the fit of the peaks around 1430 and 1542 cm^{-1} as a function of time.

Raman pump power dependence:

We conducted Raman pump power dependence where the photoexcitation pump power in these experiments was 110 μW and the Raman pump power was between 25 – 188 μW . The Raman gain of the peak around 1430 cm^{-1} at time delay of 1070 fs as a function of Raman pump power is plotted in the figure below. The linear fit below has a r^2 value of 0.996 which shows that the excited state peaks are in the linear regime with respect to the Raman pump power.

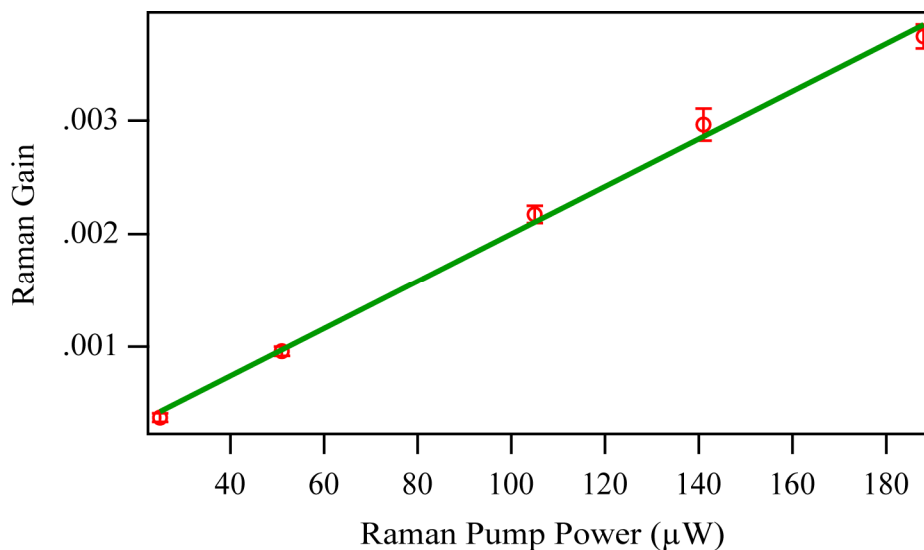


Figure S8. Raman gain with linear fit of the peak around 1430 cm^{-1} at time delay of 1070 fs.

Photoexcitation power dependence:

We conducted a photoexcitation pump power dependence where the Raman pump power was $110\ \mu\text{W}$ and the power of the photoexcitation pump was between $13.5 - 270\ \mu\text{W}$. We plot the Raman gain of the peak around 1430 cm^{-1} at time delay of 1070 fs as a function of photoexcitation pump power in the figure below. The Raman gain shows a power dependence on the photoexcitation pump power, which indicates the presence of exciton-exciton annihilation. The existence of some exciton-exciton annihilation will affect the overall triplet yield, but does not affect the observed structural dynamics that we see for the molecules that do reach the triplet state.

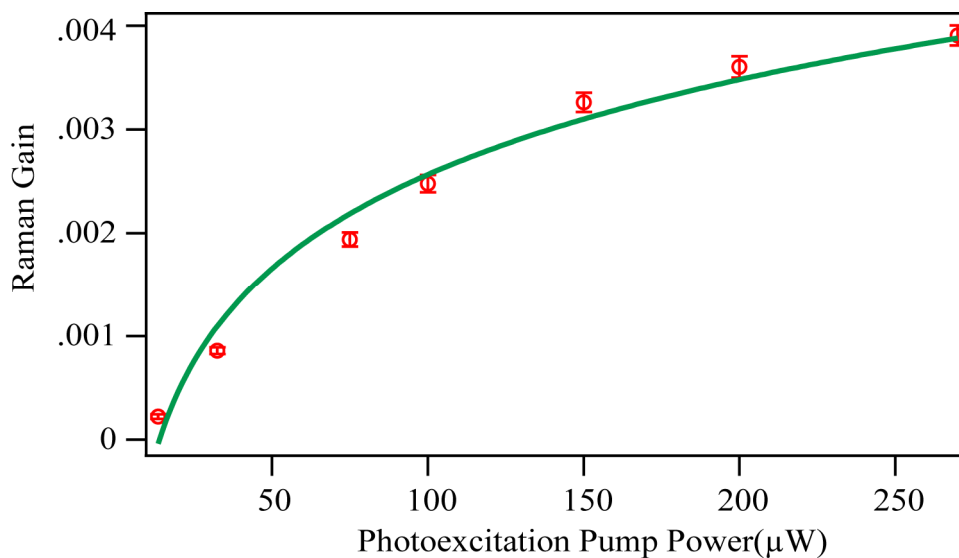


Figure S9. Raman gain with power law fit of the peak around 1430 cm^{-1} at time delay of 1070 fs.

Raman spectra of three forms of rubrene:

To probe the difference between powder and crystalline states on the fingerprint region vibrational frequencies, we measured the spontaneous Raman spectrum of rubrene single crystal, rubrene powder and rubrene solution in chloroform. From the plot below, we do not see any shift in the frequencies of the high energy vibrational modes.

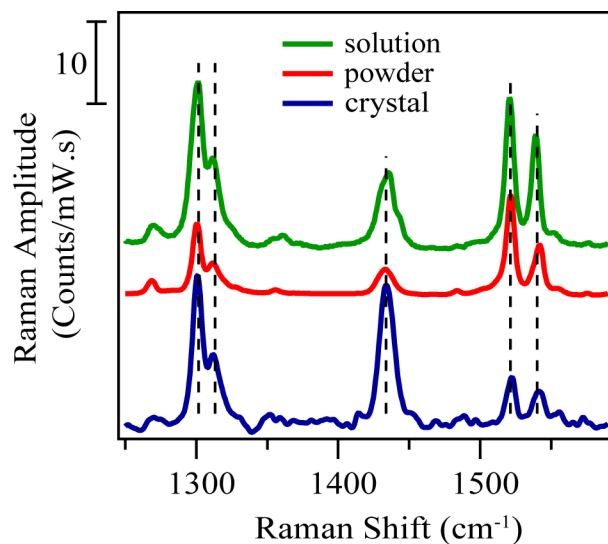


Figure S10. Spontaneous Raman spectra of rubrene single crystal, rubrene powder and rubrene solution in chloroform demonstrates that the mode frequencies do not change in the fingerprint region.

FSR data of rubrene solution in chloroform:

To verify that the features in the FSR data of crystalline rubrene arises from singlet fission, we performed FSR studies on rubrene solution in chloroform, which is known to not undergo singlet fission.⁹ We plot the FSR data after one to one subtraction of the excited state spectra from the ground state spectrum in Figure S11 and the transient absorption data in Figure S12. From the FSR and TA data below, we confirm that the interesting transient features visible in the FSR data of the crystalline rubrene arises due to singlet fission process.

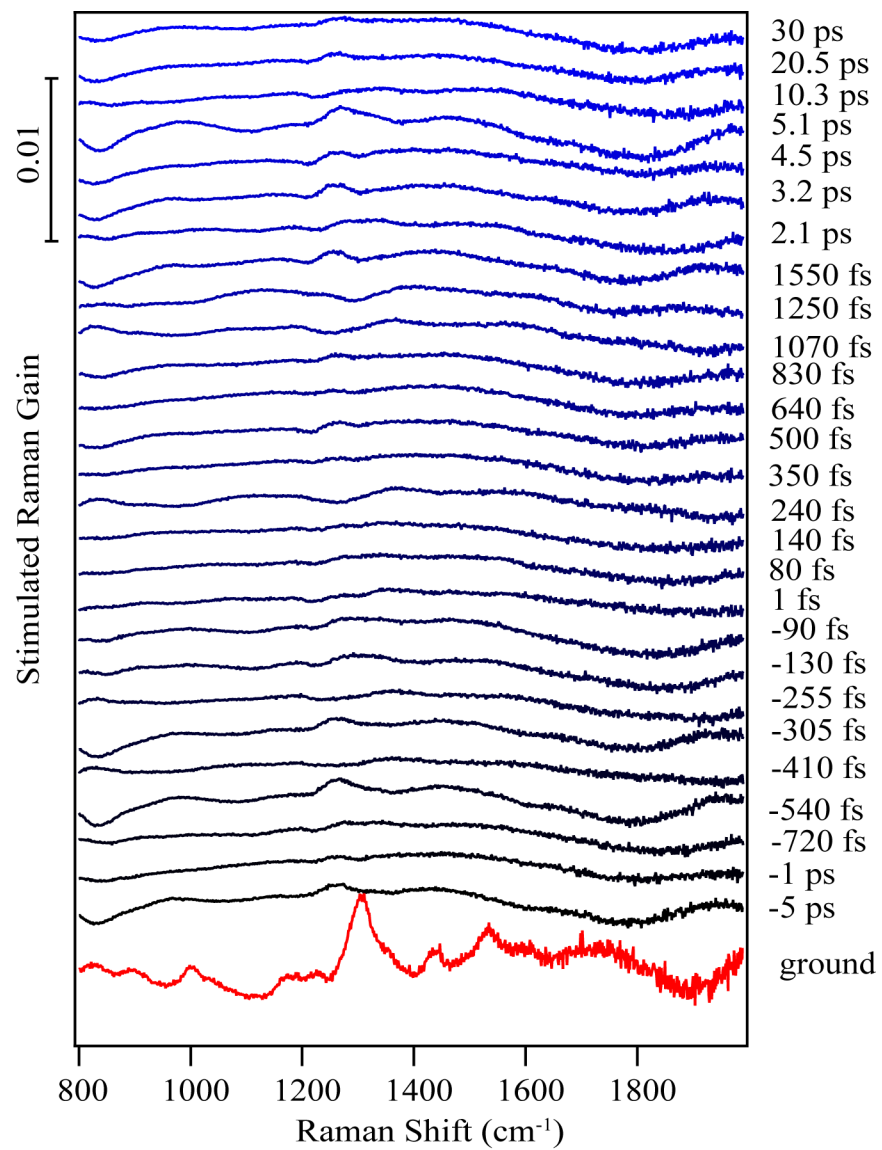


Figure S11. FSR data of rubrene solution in chloroform after one to one subtraction of the excited state spectra from the ground state spectrum.

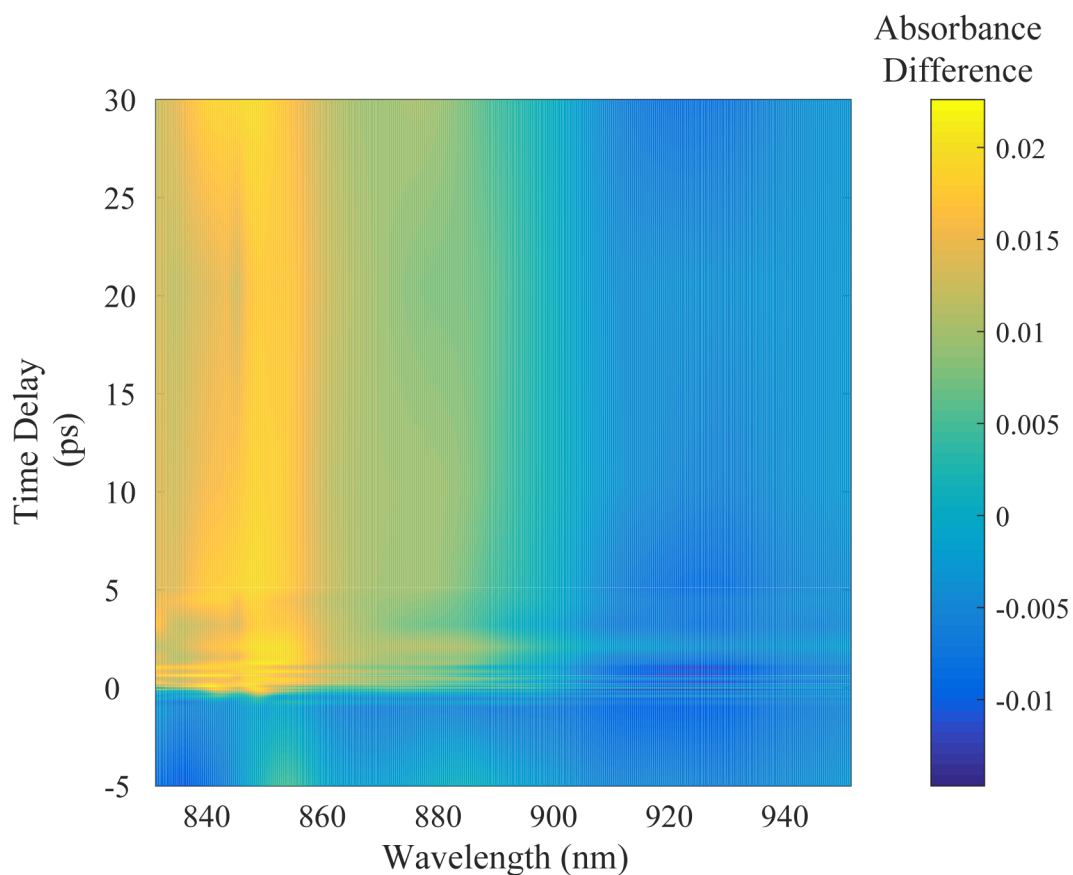


Figure S12. Transient absorption plot of rubrene solution in chloroform. The absence of 877 nm peak here confirms that the assignment of the crystalline rubrene features in the main text to dynamics resulting from singlet fission are correct.

DFT calculations:

We performed DFT calculations for the geometry optimization and Raman frequencies of neutral, anion and cation states of rubrene. Orthorhombic rubrene crystallizes with a planar tetracene backbone.^{10,11} The scaled vibrational frequencies obtained from the calculations are reported in Table 2 in the main text. The converged energy values are listed in Table S1 and the coordinates of the optimized geometries are present in Tables S2-S4.

Table S1: Calculated energies.

Rubrene state	Energy (Hartree)
Neutral	-1617.711601
Anion	-1617.763636
Cation	-1617.487549

Table S2: Optimized geometry of neutral rubrene.

Atom	X	Y	Z
C	0	0	0.73673
C	1.246764	0.103583	1.427113
C	2.431637	0.378387	0.722315
C	3.687371	0.573499	1.396573
C	4.845707	0.790501	0.711274
C	1.413312	-0.26774	2.872973
C	1.609597	0.675259	3.887569
C	1.881834	0.271375	5.192337
C	1.973538	-1.084377	5.504531
C	1.78951	-2.033185	4.500959
C	1.51482	-1.626437	3.197005
H	3.706663	0.555988	2.476286
H	5.772252	0.9516	1.251011
H	1.541614	1.731119	3.653558
H	2.021997	1.017698	5.966467
H	2.189346	-1.397283	6.520023
H	1.866484	-3.090639	4.729875
H	1.385537	-2.368107	2.416154
C	-1.246764	-0.103583	1.427113
C	-2.431637	-0.378387	0.722315
C	-3.687371	-0.573499	1.396573
C	-4.845707	-0.790501	0.711274
C	-1.413312	0.26774	2.872973
C	-1.609597	-0.675259	3.887569
C	-1.881834	-0.271375	5.192337
C	-1.973538	1.084377	5.504531
C	-1.78951	2.033185	4.500959
C	-1.51482	1.626437	3.197005
H	-3.706663	-0.555988	2.476286
H	-5.772252	-0.9516	1.251011
H	-1.541614	-1.731119	3.653558

H	-2.021997	-1.017698	5.966467
H	-2.189346	1.397283	6.520023
H	-1.866484	3.090639	4.729875
H	-1.385537	2.368107	2.416154
C	0	0	-0.73673
C	-1.246764	-0.103583	-1.427113
C	-2.431637	-0.378387	-0.722315
C	-3.687371	-0.573499	-1.396573
C	-4.845707	-0.790501	-0.711274
C	-1.413312	0.26774	-2.872973
C	-1.609597	-0.675259	-3.887569
C	-1.881834	-0.271375	-5.192337
C	-1.973538	1.084377	-5.504531
C	-1.78951	2.033185	-4.500959
C	-1.51482	1.626437	-3.197005
H	-3.706663	-0.555988	-2.476286
H	-5.772252	-0.9516	-1.251011
H	-1.541614	-1.731119	-3.653558
H	-2.021997	-1.017698	-5.966467
H	-2.189346	1.397283	-6.520023
H	-1.866484	3.090639	-4.729875
H	-1.385537	2.368107	-2.416154
C	1.246764	0.103583	-1.427113
C	2.431637	0.378387	-0.722315
C	3.687371	0.573499	-1.396573
C	4.845707	0.790501	-0.711274
C	1.413312	-0.26774	-2.872973
C	1.609597	0.675259	-3.887569
C	1.881834	0.271375	-5.192337
C	1.973538	-1.084377	-5.504531
C	1.78951	-2.033185	-4.500959
C	1.51482	-1.626437	-3.197005
H	3.706663	0.555988	-2.476286
H	5.772252	0.9516	-1.251011
H	1.541614	1.731119	-3.653558
H	2.021997	1.017698	-5.966467
H	2.189346	-1.397283	-6.520023
H	1.866484	-3.090639	-4.729875
H	1.385537	-2.368107	-2.416154

Table S3: Optimized geometry of rubrene anion.

Atom	X	Y	Z
C	0	0	0.737126
C	1.247514	0.094931	1.42089
C	2.450071	0.408771	0.721439
C	3.690272	0.631481	1.3874
C	4.86427	0.873315	0.70315
C	1.400257	-0.347852	2.844269
C	1.69172	0.521559	3.904526
C	1.927381	0.040781	5.190886
C	1.882566	-1.328282	5.450605
C	1.597194	-2.209349	4.407985
C	1.361399	-1.722399	3.124372
H	3.714825	0.605833	2.467962
H	5.78391	1.048369	1.252885
H	1.719282	1.588674	3.716679
H	2.138937	0.738973	5.994563
H	2.065867	-1.703102	6.452404
H	1.563592	-3.278752	4.59284
H	1.148189	-2.411615	2.314509
C	-1.247514	-0.094931	1.42089
C	-2.450071	-0.408771	0.721439
C	-3.690272	-0.631481	1.3874
C	-4.86427	-0.873315	0.70315
C	-1.400257	0.347852	2.844269
C	-1.69172	-0.521559	3.904526
C	-1.927381	-0.040781	5.190886
C	-1.882566	1.328282	5.450605
C	-1.597194	2.209349	4.407985
C	-1.361399	1.722399	3.124372
H	-3.714825	-0.605833	2.467962
H	-5.78391	-1.048369	1.252885
H	-1.719282	-1.588674	3.716679
H	-2.138937	-0.738973	5.994563
H	-2.065867	1.703102	6.452404
H	-1.563592	3.278752	4.59284
H	-1.148189	2.411615	2.314509
C	0	0	-0.737126
C	-1.247514	-0.094931	-1.42089
C	-2.450071	-0.408771	-0.721439
C	-3.690272	-0.631481	-1.3874
C	-4.86427	-0.873315	-0.70315
C	-1.400257	0.347852	-2.844269

C	-1.69172	-0.521559	-3.904526
C	-1.927381	-0.040781	-5.190886
C	-1.882566	1.328282	-5.450605
C	-1.597194	2.209349	-4.407985
C	-1.361399	1.722399	-3.124372
H	-3.714825	-0.605833	-2.467962
H	-5.78391	-1.048369	-1.252885
H	-1.719282	-1.588674	-3.716679
H	-2.138937	-0.738973	-5.994563
H	-2.065867	1.703102	-6.452404
H	-1.563592	3.278752	-4.59284
H	-1.148189	2.411615	-2.314509
C	1.247514	0.094931	-1.42089
C	2.450071	0.408771	-0.721439
C	3.690272	0.631481	-1.3874
C	4.86427	0.873315	-0.70315
C	1.400257	-0.347852	-2.844269
C	1.69172	0.521559	-3.904526
C	1.927381	0.040781	-5.190886
C	1.882566	-1.328282	-5.450605
C	1.597194	-2.209349	-4.407985
C	1.361399	-1.722399	-3.124372
H	3.714825	0.605833	-2.467962
H	5.78391	1.048369	-1.252885
H	1.719282	1.588674	-3.716679
H	2.138937	0.738973	-5.994563
H	2.065867	-1.703102	-6.452404
H	1.563592	-3.278752	-4.59284
H	1.148189	-2.411615	-2.314509

Table S4: Optimized geometry of rubrene cation.

Atom	X	Y	Z
C	0	0	0.735228
C	1.241161	0.084971	1.430868
C	2.437196	0.386799	0.718565
C	3.670829	0.59874	1.394359
C	4.832238	0.858891	0.703752
C	1.395687	-0.326314	2.86059
C	1.683841	0.574594	3.892371
C	1.92865	0.111725	5.181906
C	1.913491	-1.256017	5.454083
C	1.642185	-2.160079	4.42996

C	1.380541	-1.699099	3.141884
H	3.695755	0.55773	2.472865
H	5.752641	1.03911	1.246306
H	1.696388	1.639267	3.691015
H	2.133924	0.821111	5.975148
H	2.114966	-1.613163	6.457179
H	1.637712	-3.225482	4.62968
H	1.180507	-2.40892	2.346739
C	-1.241161	-0.084971	1.430868
C	-2.437196	-0.386799	0.718565
C	-3.670829	-0.59874	1.394359
C	-4.832238	-0.858891	0.703752
C	-1.395687	0.326314	2.86059
C	-1.683841	-0.574594	3.892371
C	-1.92865	-0.111725	5.181906
C	-1.913491	1.256017	5.454083
C	-1.642185	2.160079	4.42996
C	-1.380541	1.699099	3.141884
H	-3.695755	-0.55773	2.472865
H	-5.752641	-1.03911	1.246306
H	-1.696388	-1.639267	3.691015
H	-2.133924	-0.821111	5.975148
H	-2.114966	1.613163	6.457179
H	-1.637712	3.225482	4.62968
H	-1.180507	2.40892	2.346739
C	0	0	-0.735228
C	-1.241161	-0.084971	-1.430868
C	-2.437196	-0.386799	-0.718565
C	-3.670829	-0.59874	-1.394359
C	-4.832238	-0.858891	-0.703752
C	-1.395687	0.326314	-2.86059
C	-1.683841	-0.574594	-3.892371
C	-1.92865	-0.111725	-5.181906
C	-1.913491	1.256017	-5.454083
C	-1.642185	2.160079	-4.42996
C	-1.380541	1.699099	-3.141884
H	-3.695755	-0.55773	-2.472865
H	-5.752641	-1.03911	-1.246306
H	-1.696388	-1.639267	-3.691015
H	-2.133924	-0.821111	-5.975148
H	-2.114966	1.613163	-6.457179
H	-1.637712	3.225482	-4.62968
H	-1.180507	2.40892	-2.346739
C	1.241161	0.084971	-1.430868
C	2.437196	0.386799	-0.718565
C	3.670829	0.59874	-1.394359

C	4.832238	0.858891	-0.703752
C	1.395687	-0.326314	-2.86059
C	1.683841	0.574594	-3.892371
C	1.92865	0.111725	-5.181906
C	1.913491	-1.256017	-5.454083
C	1.642185	-2.160079	-4.42996
C	1.380541	-1.699099	-3.141884
H	3.695755	0.55773	-2.472865
H	5.752641	1.03911	-1.246306
H	1.696388	1.639267	-3.691015
H	2.133924	0.821111	-5.975148
H	2.114966	-1.613163	-6.457179
H	1.637712	-3.225482	-4.62968
H	1.180507	-2.40892	-2.346739

References:

- (1) Laudise, R. A.; Kloc, C.; Simpkins, P. G.; Siegrist, T. Physical Vapor Growth of Organic Semiconductors. *J. Cryst. Growth* **1998**, *187*, 449–454.
- (2) Reyes-Martinez, M. A.; Ramasubramaniam, A.; Briseno, A. L.; Crosby, A. J. The Intrinsic Mechanical Properties of Rubrene Single Crystals. *Adv. Mater.* **2012**, *24*, 5548–5552.
- (3) Ogden, W. A.; Ghosh, S.; Bruzek, M. J.; McGarry, K. A.; Balhorn, L.; Young, V.; Purvis, L. J.; Wegwerth, S. E.; Zhang, Z.; Serratore, N. A.; *et al.* Partial Fluorination as a Strategy for Crystal Engineering of Rubrene Derivatives. *Cryst. Growth Des.* **2017**, *17*, 643–658.
- (4) Silva, W. R.; Frontiera, R. R. Excited State Structural Evolution during Charge-Transfer Reactions in Betaine-30. *Phys. Chem. Chem. Phys.* **2016**, *18*, 20290–20297.
- (5) McCamant, D. W.; Kukura, P.; Yoon, S.; Mathies, R. A. Femtosecond Broadband Stimulated Raman Spectroscopy: Apparatus and Methods. *Rev. Sci. Instrum.* **2004**, *75*, 4971–4980.
- (6) Venuti, E.; Bilotti, I.; Valle, R. G. D.; Brillante, A.; Ranzieri, P.; Masino, M.; Girlando, A. Polarized Raman Spectra of a Rubrene Single Crystal. *J. Phys. Chem. C* **2008**, *112*, 17416–17422.
- (7) Ma, L.; Zhang, K.; Kloc, C.; Sun, H.; Soci, C.; Michel-Beyerle, M. E.; Gurzadyan, G. G. Fluorescence from Rubrene Single Crystals: Interplay of Singlet Fission and Energy Trapping. *Phys. Rev. B - Condens. Matter Mater. Phys.* **2013**, *87*, 1–5.
- (8) Chen, Y.; Lee, B.; Fu, D.; Podzorov, V. The Origin of a 650 nm Photoluminescence Band

- in Rubrene. *Adv. Mater.* **2011**, *23*, 5370–5375.
- (9) Ma, L.; Zhang, K.; Kloc, C.; Sun, H.; Michel-Beyerle, M. E.; Gurzadyan, G. G. Singlet Fission in Rubrene Single Crystal: Direct Observation by Femtosecond Pump–probe Spectroscopy. *Phys. Chem. Chem. Phys.* **2012**, *14*, 8307–8312.
- (10) Paraskar, A. S.; Reddy, A. R.; Patra, A.; Wijsboom, Y. H.; Gidron, O.; Shimon, L. J. W.; Leitus, G.; Bendikov, M. Rubrenes: Planar and Twisted. *Chem. - A Eur. J.* **2008**, *14*, 10639–10647.
- (11) McGarry, K. A.; Xie, W.; Sutton, C.; Risko, C.; Wu, Y.; Young, V. G.; Brédas, J. L.; Frisbie, C. D.; Douglas, C. J. Rubrene-Based Single-Crystal Organic Semiconductors: Synthesis, Electronic Structure, and Charge-Transport Properties. *Chem. Mater.* **2013**, *25*, 2254–2263.